

The Effect of Curing Time on Electrical Resistivity, Mechanical Characteristics and Microstructure Behavior of Graphene Conductive Ink

Ameeruz Kamal Ab Wahid¹, Mohd Azli Salim^{1,2,3*}, Nor Azmami Masripan^{1,2,3}, Murni Ali⁴, Adzni Md. Saad^{1,3}, and Mohammed Hussin A. Al-Mola⁵

¹Fakulti Kejuruteraan Mekanikal, Universiti Teknikal Malaysia Melaka, Hang Tuah Jaya, 76100 Durian Tunggal, Melaka, Malaysia

²Advanced Manufacturing Centre, Universiti Teknikal Malaysia Melaka, Hang Tuah Jaya, 76100 Durian Tunggal, Melaka, Malaysia

³Intelligent Engineering Technology Services Sdn. Bhd., No.1, Jalan TU43, Taman Tasik Utama, 76450 Ayer Keroh, Melaka, Malaysia

⁴NanoMalaysia Berhad, A-2-3, Level 2, 157 Hampshire Place Office No. 1, Jalan Mayang Sari, 50450 Kuala Lumpur.

⁵Faculty of Petroleum and Mining Engineering, University of Mosul, Mosul, Iraq.

ABSTRACT

Nowadays graphene conductive ink (CI) are expected to be widely used for various automotive safety electronic equipment in the future. Graphene has a potential advantage such as high electrical conductivity and thermal conductivity and can be applied to electronic circuits in vehicles especially for driver health monitoring systems. To ensure optimal conductivity, graphene need to go through a curing process to minimize porosity between particles and create a smooth conductive track. The effect of curing time on electrical, mechanical, and microstructural properties was investigated. Five samples at 20 wt.% filler loading with curing times varying from 10-50 minutes with each sample interval of 10 minutes was executed using doctor-blading printing method before analysis. Then, the analysis is done by using four-point probe to measure resistance, followed by nano-indentation and scanning electron microscope (SEM) to study elasticity and observe microstructure behaviour respectively with respect to temperature. Sample of 30 minutes curing time gives the lowest result, 24.9046 $\Omega \cdot \text{cm}$ for volume of resistivity. The sample also has excellent mechanical properties, with high Young's modulus and low hardness, 8.59 GPa and 7.59 MPa respectively. Stretchable conductive ink (SCI) in vehicle electronic equipment with low resistance and high elasticity can monitor the driver's health more effectively because it can be stretched to fit the shape of the human body. It also has good conductivity for measuring human pulse and muscle movement.

KEYWORDS: Stretchable conductive ink, graphene formulation, resistivity, elasticity, curing times

1. INTRODUCTION

Nowadays the development of CI among electronic users is increasing rapidly. Printed electronics technology originally to emerge as a potential low-cost replacement to its complementary technology, silicon-based electronics. As the substrates grow thinner, it is enough to be integrated into existing production lines because the printed materials become thin, light, and flexible. SCI is characterised by its flexibility and expandability while maintaining low resistivity levels. Stretchability benefits from low resistance changes [1]. Printed electronics objectives are not only to be cheaper alternatives by replacing the individual electronic layers but also to develop complex materials that deliver additional functionalities which a two-

*Corresponding Author: azli@utem.edu.my

component solution that controlling the viscosity can be used to produce a self-assembled structure based on the affinity of the solution components to each other [2].

A standard driver health monitoring system is set up to continuously track parameters relevant to drivers, cars, and the environment using data collected from a variety of sensors on the driver's body, interior, and exterior of the vehicle. Due to the detection of mechanical pressure and strain, temperature variations, and bio-potential changes in the human body, various types of drivers produce different outcomes.

Graphene is an increasingly widely used CI in flexible electronic equipment and becomes a major source of research with many desirable properties including high electrical conductivity, mechanical strength, and elasticity [3]. The available screen-printed CI when this research started exhibits very limited stretchability and cannot be used in applications that require flexibility and stretchability. One major challenge of graphene CI is to formulate a suitable ink formulation that can be printed using doctor-blading-based methods. The development of graphene-based inks is mainly focusing on the relevant material, ink preparation, and optimization of conductivity. Because of the strong van der Waals forces between adjacent layers, the graphene sheets are inherently stacked together. Then, it is difficult to exfoliate and distribute graphite nanosheets evenly into a polymer matrix [4].

An experimental investigation was conducted to explore suitable graphene formulation of the curing times, electrical resistivity, elasticity, hardness and microstructure. The fluidic properties of graphene inks, such as filler, solvent, and additives, necessitate specific viscosity and surface tension. It enables the use of existing instrumentation to print inks with low volatilizing temperatures and high adhesion to layers. These characteristics allow the inks to be used on a variety of substrates, demonstrating their superior flexibility and stretchability [5].

2. EXPERIMENTAL METHODS

2.1 Preparation of Graphene CI Formulation

The key materials for this research were Graphene nanoplatelets powder (GNP) as a filler ingredient, Araldite as an epoxy resin, and Polytheramine as a hardener, which were used without further alteration. The thinky mixer unit was used to mix all of the raw materials (GNP, epoxy, and hardener). Because of its low cost and high electrical conductivity, graphene is a suitable filler element for industrial-scale processing [6]. Table 1 lists the GNP properties that can be found on the product datasheet.

Table 1 Properties of GNP

Specification	
Form	Powder
Surface area	50-80 m ² /g
Average flake thickness	15 nm
Average particle size	5 μm
Density	0.03 – 0.1 g/cm ³

Araldite was an embedding epoxy resin. Araldite, dodecenyl succinic anhydride, dibutyl phthalate, and 2, 4, 6-tridimethylamine methyl phenol are the main ingredients of the epoxy resin, which is colorless. To harden or dry the solution mixtures, polytheramine was used as a hardener. The hardener is a liquid material that is used to keep the viscosity of CI consistent in

all printing processes. Polytheramine is a curing agent in the amine group that produces durable, transparent coatings, castings, and adhesives.

The formulation materials for the experiments were prepared and added accordingly to the predefined ratio inside a container starting with GNP powder. The formulations contained 0.5 g of resin and hardener. As shown in Table 2, the sample of graphene filler loading is using same formulation, 20 wt.% of graphene mixing with 80 wt.% of binder (epoxy) and hardener (30% of epoxy weight). The formulation chosen is based on previous experiments findings which filler loading percentages, 20 wt.% gives the best resistivity, Young's modulus and hardness values, 24.9046 Ω .cm, 8.59 GPa and 7.59 MPa respectively [7].

The added materials were precisely weighed using the thinky mixer machine, and then mixed for three minutes at a rotational speed of 2000 rpm. The invisible micron-sized bubbles were also removed using the thinky mixer. The raw graphite materials are directly exfoliated into graphene with the help of shear mixing in liquid media. Its benefits include a low cost, the solution's ability to process, and the high conductivity of the resulting footprints [5].

A microscope glass slide with a size of 2.54 cm x 7.62 cm and a thickness of 0.1 cm - 0.12 cm was used as a substrate for the CI in this study. Because of their thermal stability over a wide temperature range and high insulation properties, glass substrates were used in the experiment to measure electrical conductivity [8].

Table 2 Formulation of the materials in the development of the conductive ink

Sample	GNP		Epoxy		Hardener (g)
	(wt.%)	(g)	(wt.%)	(g)	
20wt.%	20	0.100	80	0.400	0.120

As shown in Figure 1 below, the schematic of printed patterns of thick layer dimensions of 3.0 mm (width, w) x 25.4 mm (length, l) x 0.1 mm (thickness, t_s) were printed on the glass slide. The samples were prepared precisely according to every applicable test to evaluate certain characterizations.

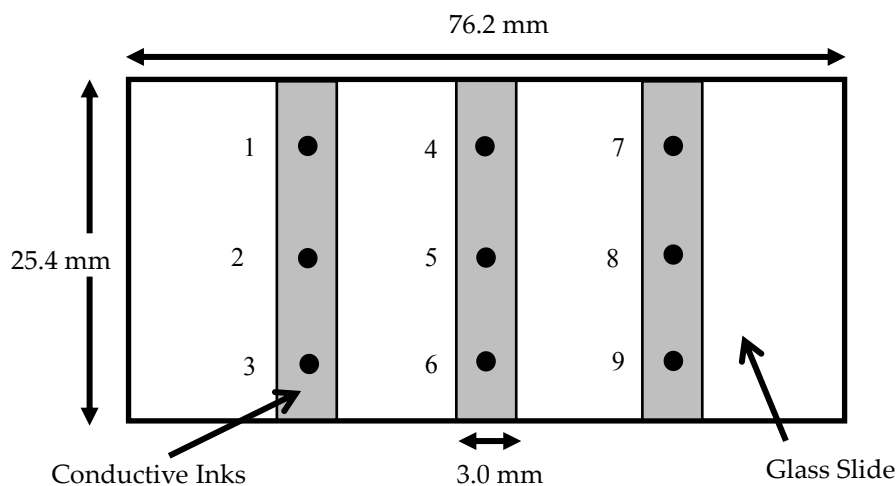


Figure 1. Schematic of printed CI on a glass slide with 9 marking points for electrical measurement.

The commonly used method for the curing process is heating in an oven. The sample was placed in an oven and set at an appropriate temperature and time to avoid damaging the formulated

material and substrates. This method used at low temperatures also helped in reducing the time of the curing and also diversifying the types of substrates that can be used [9]. Several studies had been carried out to find the low sheet resistance, which is time-consuming and not economically viable for mass production [6].

The main objective of the curing time experiment is to find the finest curing time for the filler loading and to see how different curing times affect graphene filler loading. The time for curing will be done from 10-50 minutes with each sample interval of 10 minutes. The sample will be tested for electrical and mechanical behavior characteristics. An experimental investigation also was conducted to explore suitable curing time for the graphene formulation resistivity, elasticity, and microstructure delamination.

After the curing process, the following process was normalizing all specimens at room temperature for about 24 hours and then, the specimen was placed inside the desiccator. Normalizing is the process of heating a material to a temperature above a critical limit and then cooling it in the open air. The objective of normalizing the heat temperature is to improve the material's mechanical properties by optimizing the microstructure.

2.3 Volume of Resistivity Measurement

The main objective of this experiment is to determine whether electrical conductivity can be used in circuits using CI. The resistance of the material used to construct the circuit determines its electrical conductivity. The materials used to produce a circuit are a mix of materials with varying percentages. The different curing times in the formulations result in different sheet resistance values. As shown in Figure 3, the samples were measured using a four-terminal (4T) sensing method at room temperature with an input range of 10 nA to 100 mA at three different locations per stripe, resulting in 9 data per sample. The data was then used to calculate a volume of resistivity for all thick layer samples, which was then translated into a single average value.

2.4 Mechanical Characterization

The importance of mechanical properties, that are just as important as electrical properties in determining the material's strength and durability. A nano-indentation machine was used to measure the hardness of CI samples. To prevent cracking and rupture of the formulation, as well as a loss of protective effect, the nano-indentation depth must be carefully calibrated [10]. All samples were measured with a 150 mN nano-indentation force to determine the acceptable elasticity modulus. The average values taken at three different points on the sample surface were used to calculate the elasticity of this experiment.

A typical indentation experiment in this experiment includes the following steps: (1) approaching the surface, (2) loading to 150 mN peak load, (3) keeping the indenter at peak load for 5 s, (4) unloading from 150 mN maximum force, and (5) completing the unloading procedure. Since the unloading curve was used to obtain the elastic modulus of the material, the holding phase was included to avoid the effect of creep on the unloading characteristics. The form of the hardness impression after the indenter is unloaded and the material elastically recovers is one of the most important findings from this experiment. Equal loadings have made a significant and stable contribution to nanomechanical properties in nanocomposite materials [11].

2.5 Microstructure Observation

Scanning electron microscope (SEM) and energy dispersive x-ray (EDX) observations were used to describe the microstructure of the GNP formulations curing time at room temperature. To obtain the cross-section morphology view, all samples were placed together with epoxy and coated with platinum (Pt) using a SEM coating device. The gaps (dark holes) between the nanoplatelets reduce contact quality because electrons migrate through the gaps between the nanoplatelets, causing large sheet resistance between the edges and tips of the nanoplatelets [6]. The adhesion between the Nano-platelets determines the microstructure characteristics of the samples. The various SEM and EDX studies carried out in this section are discussed, as well as how they contributed to the formulation of recommendations for the CI filler loading curing time differences.

3. RESULTS AND DISCUSSION

3.1 Electrical Characterization Analysis

The measurements of resistivity (average sheet resistance, the average volume of resistivity and standard deviation values) of different curing time of filler loading percentage are presented in Table 3. The loss modulus is high for both curing time 10 of graphene than the storage modulus throughout the range of stresses measured, indicating that these formulations display liquid-like behavior [12] due to curing time that is not long enough. Results for samples curing time 20 (10.5252×10^3 R/sq) and 40 (10.9785×10^3 R/sq) do not show a significant difference between the results as the material changes to become more cohesive and increasingly fragile respectively. It makes the samples to possess less liquidity behavior and more brittle after the curing process. The results are better than what is shown in the Figure 2 [13] for graphene CI that using DMF to stabilize the graphene ink and not screen printed with sheet resistance of 2×10^5 R/sq.

Table 3 Measurement of resistivity on different curing time

Curing Time (minutes)	Sheet Resistance, Average (R/sq)	Volume of Resistivity, Average (Ω .cm)	Standard Deviation (Ω .cm)
10	12.1871×10^3	72.6134	15.6562
20	10.5252×10^3	62.7116	13.622
30	4.1799×10^3	24.9046	4.4328
40	10.9785×10^3	65.4121	8.1885
50	15.1584×10^3	90.3167	23.6626

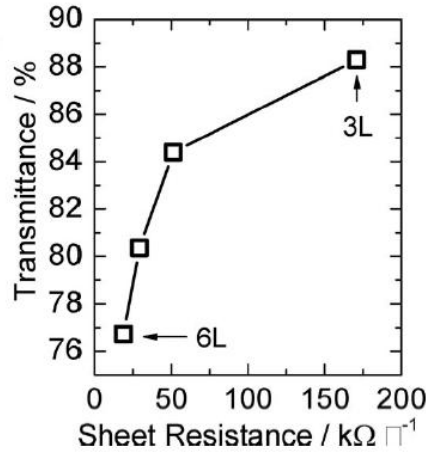


Figure 2. Graphene sheet resistance [13].

Table 3 shows the difference in volume of resistivity between different curing times ranging from 10 to 50 minutes. It also can be seen from Figure 5 when 20 and 30 minutes of curing time showed a decline in volumes of resistivity and rose after 40 and 50 minutes. This occurs due to the filler particle loading is becoming increasingly fragile and cause cracks in the material further increase the volume of resistivity. The resistance of graphene-based decreases with the increase of temperature due to the thermal annealing of graphene flakes and the removal of residual solvents and surfactants [14]. The decrease in volume of resistivity is due to graphene materials becoming more initiate as the temperature increases [15]. The increase in volume of resistivity caused by the filler loading particle became increasingly fragile, resulting in a fracture. The optimum temperature for the lowest resistance varies with curing time, with higher curing time resulting in lower optimum curing temperature [16].

From the results in Table 3, the result shows that a large difference of the value for standard deviation between curing time sample of 50 minutes to the other samples. It is because, the curing time at 50 minutes had gone through too long a burning time compared to the other samples. this also results in the graphene filler loading becoming increasingly brittle and making it unstable. Figure 3 shows that sample curing time 30 minutes have smallest standard deviation value because the percentage of graphene can balance the entire pattern on the sample. It causes the resistance of the whole pattern does not have a significant difference.

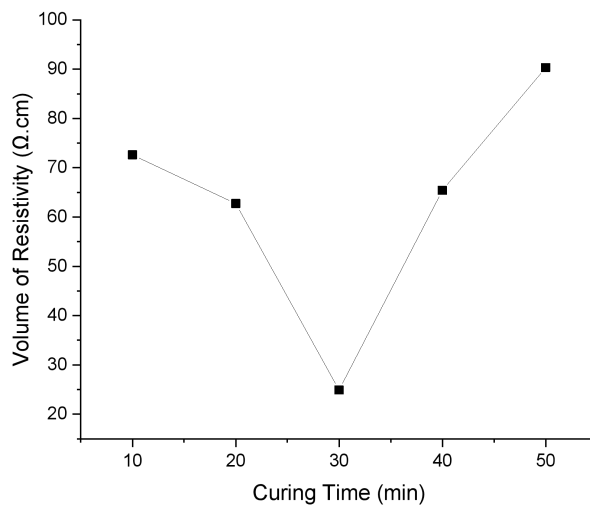


Figure 3. Volume of resistivity ($\Omega.cm$) on different curing time.

3.2 Mechanical Characterization Analysis

The hardness and elastic modulus were calculated from the recorded load-displacement curves using [17] method. Mechanical properties were directly determined by the indentation load and displacement measurements without the need to capture the image of hardness impression. The load was measured as a function of penetration depth. 150 mN nano-indentation force was tested on all five curing time samples begin with 10 until 50 minutes.

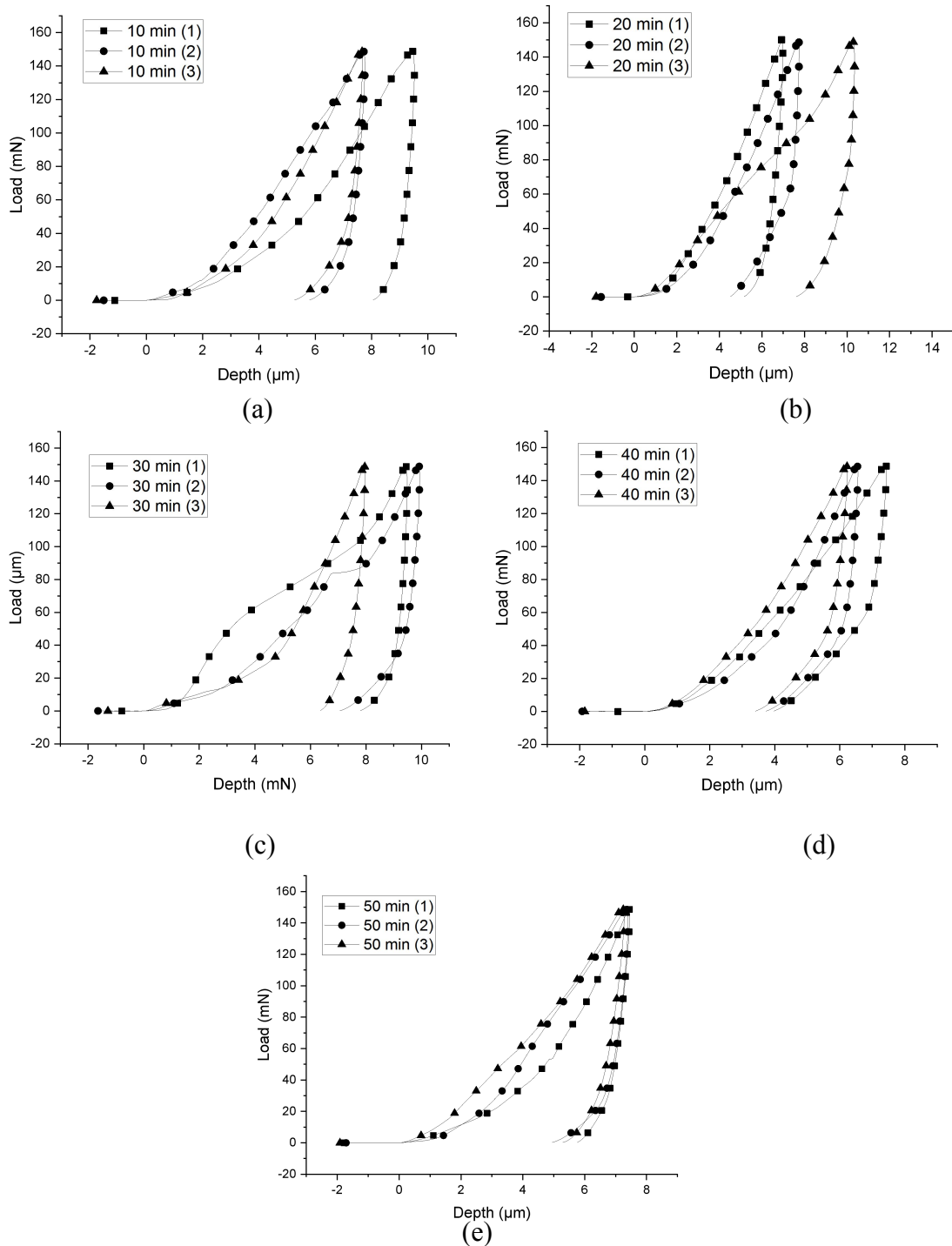


Figure 4. Representation of load–displacement curves showing different penetration depths, (a) 10 minutes, (b) 20 minutes (c) 30 minutes, (d) 40 minutes, (e) 50 minutes.

For each sample of filler loading surface, Figures 4(a,b,c,d,e) indicate three different indentation points. The three points are used to assess the uniformity of penetration depth for various filler loading percentages in relation to hardness and Young's modulus. To remove the viscoelastic contribution and prove the [17] model, a nano-indentation test was performed with a maximum force of 150 mN and a retention time of 5 s. The curing time 30 minutes sample has the highest penetration depth, as shown by the load-displacement curves in Figure 4. In the reinforced samples, the resistance to displacement of GNP at curing time 30 minutes has the highest plastic strain endurance as compared to the other filler loading curing times.

The result shows in Table 4 is taken based on the average of the three different points on the sample surface. The average values of hardness and Young's modulus depending on the nanofiller concentration obtained from nano-indentation tests over a different curing times of CI filler loading are presented in Figures 6(a,b). The result shows that the average Young's modulus and average hardness are within the range 7.664 to 8.862 GPa and 7.59 to 14.455 MPa respectively. The results are better than what is shown in Figure 7 [11] for nano-indentation experimental of graphene CI that using 1 to 12 wt.% filler loading with indentation maximum force of 100 mN with Young's modulus and hardness results of 3.5 to 3.75 GPa and 175 to 200 MPa respectively.

Table 4 Nano-indentation results of different curing times

Curing Times (minutes)	Average Maximum Depth, h_{max} (μm)	Average Young's Modulus, E (GPa)	Young's Modulus Standard Deviation (GPa)	Average Hardness, HV (MPa)	Hardness Standard Deviation (MPa)
10	8.264	7.664	1.600	9.337	2.128
20	8.312	7.82	1.687	9.787	3.767
30	9.095	8.59	1.41	7.59	1.92
40	6.723	8.862	2.502	14.455	2.517
50	7.337	7.735	1.261	11.805	0.492

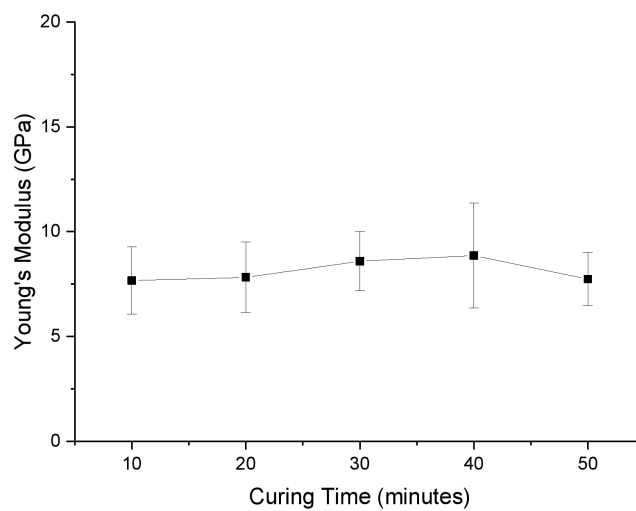


Figure 5. Mean values of filler loading curing time Young's modulus.

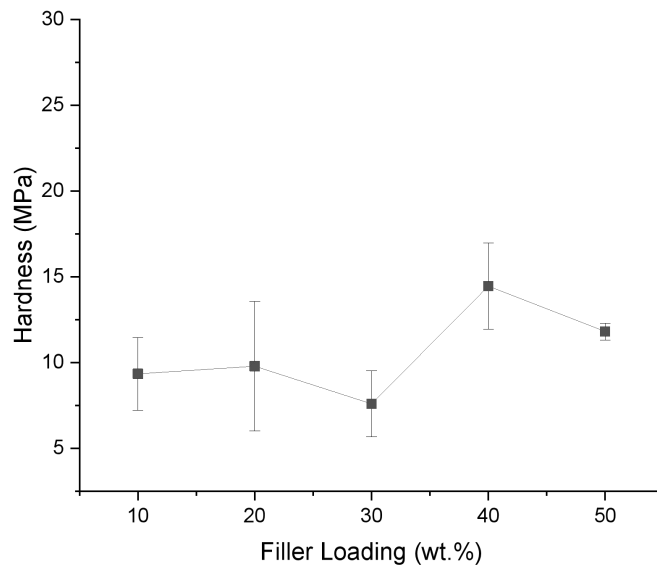


Figure 6. Mean values of filler loading curing time hardness.

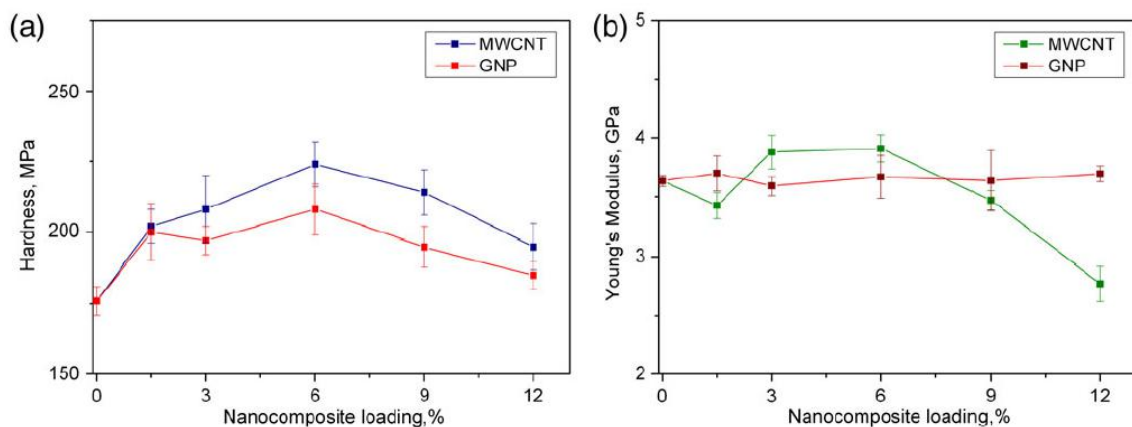


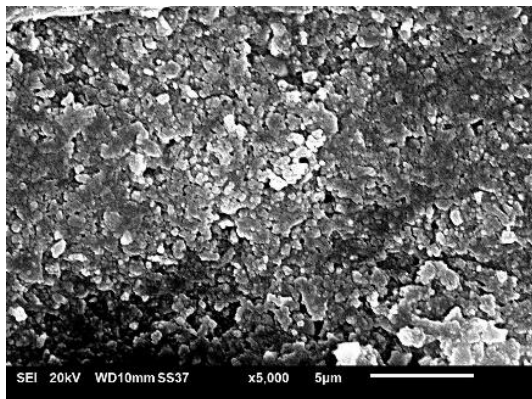
Figure 7: Mean values of (a) hardness and (b) Young's modulus of elasticity versus mono-filler content [11].

The results show in Figures 5 and Figure 6 for hardness and elasticity respectively have the highest standard deviations for 30 minutes curing times as compared to the other samples. The level of dispersion of the experimental results is significant for the sensibility of the indenter to the inhomogeneity of the composite structure with different percentages of GNP. The experimental errors are within the range ± 1.261 to ± 2.502 GPa for Young's modulus and ± 0.492 to ± 3.767 MPa for hardness. It can be observed that 30 minutes curing times of GNP in the filler loading matrix is giving the best results for nano-mechanical properties. It is because the filler loading is uniformly dispersed in the CI matrix and no obvious aggregation is observed. The low values for 10 minutes curing times filler loading mono-filled nanocomposites can be explained with the formation of aggregates in the CI structure, resulting in the worst carbon nanofiller dispersion and therefore having low hardness and elasticity. The resistance to displacement of 10 minutes curing times comparing to 30 minutes curing times of filler loading suggests the higher endurance to plastic strain in the reinforced samples.

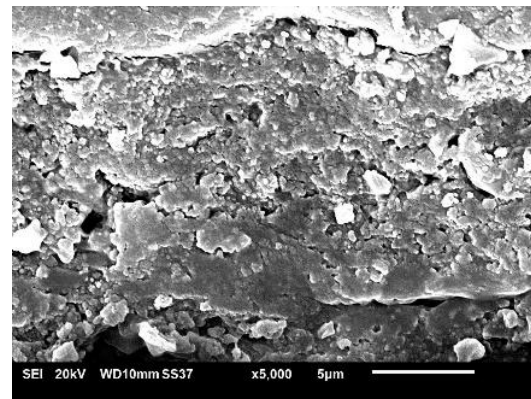
3.3 Microstructure Analysis

Figure 8(a,b,c,d,e) shows the cross-sectional view structure of carbon nanofillers in the CI using SEM images of the filler loading percentages. It also indicates that all samples have the same particle size distribution, which is 5 microns. The cross-section view SEM tests of 10 to 50 minutes of curing times showed that the 30 minutes curing time samples filler loading CI are more densely packed than the other samples. This is shown by the lack of cracking on the cross-sectional surface after 30 minutes of curing time. The GNP filler loading curing times result in the formation of a contact network in the mixture, and also to well-dispersed carbon nanofillers. The microstructure also has a denser structure when the temperature is raised since the void between particles is reduced [15].

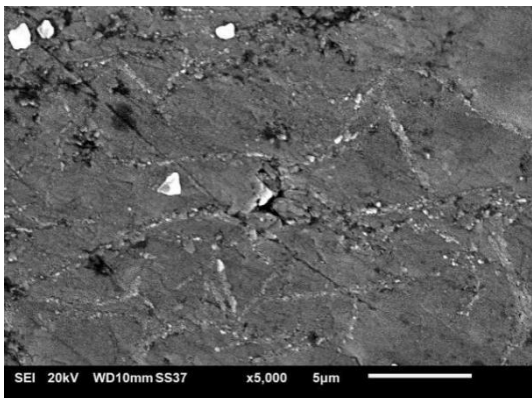
Comparative SEM images are very helpful in determining conductivity and understanding ink behavior. Figure 8 shows the comparative SEM images of the 10 to 50 minutes curing times of graphene filler loading. In Figure 8 observation, the 30 minutes curing times of filler loading are more homogeneous because it has a more solid structural shape than the other samples. 10 minutes curing time filler loading had the most cracks compared to the other samples. The brittleness of the filler loading increases as the curing time increases, resulting in possible cracks in the cross-section of CI.



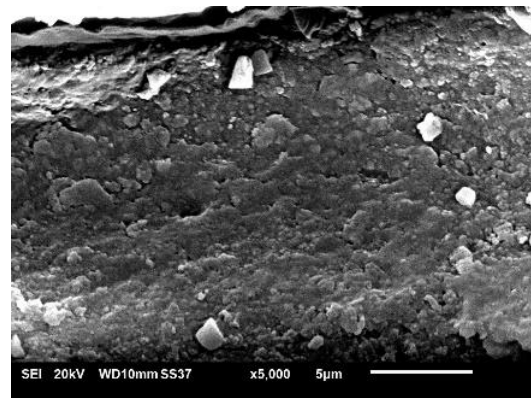
(a)



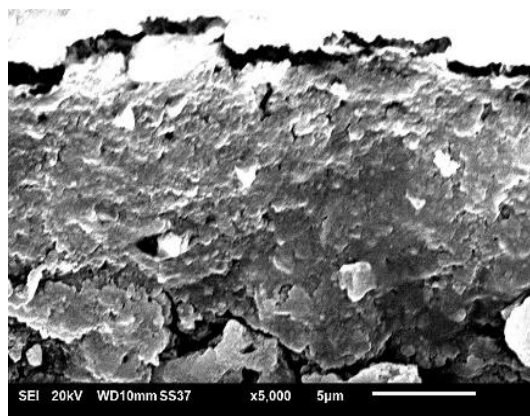
(b)



(c)



(d)



(e)

Figure 8. SEM images of filler loading cross-section area on different curing time, (a) 10 minutes, (b) 20 minutes, (c) 30 minutes, (d) 40 minutes and (e) 50 minutes.

3.4 EDX Analysis to Validate SEM Images of CIs

Table 5 shows that the 10 minutes curing times has a lowest weight percentage of carbon (graphene), 62.47% compared to others filler loading percentage of graphene. Generally, the higher the graphene content, the more brittle is the graphene and that would lead to higher cracks and loss in conductivity during straining [18].

The cross-section characteristics of the CI were correlated with their material properties, assessing the components of the materials by SEM and EDX analysis (SEM–EDX). The presence of carbon (C) was found in the five tested CIs. The release of carbon is important because it plays a role in conductivity, and in addition to that because it is responsible for the resistivity of the material. The EDX results in Table 5 gave different results for filler loading in terms of percentage of weight. EDX showed peaks of carbon (C) and oxygen (O) in the materials, but in different percentages.

Table 5 Weight and atomic percentages of filler loading elements

Curing Time (minutes)	Weight (%)			Atomic (%)		
	Carbon, C	Oxygen, O	Total	Carbon, C	Oxygen, O	Total
10	62.47	37.53		67.81	32.19	
20	65.33	34.67		71.51	28.49	
30	67.95	32.05	100%	72.98	27.02	100%
40	69.09	30.91		74.86	25.14	
50	72.52	27.48		77.85	22.15	

The presence of oxygen content is because the graphene molecules disrupts the hydrogen bonding exist in epoxy and forms a strong molecular interaction with the residual oxygen found on graphene tail [19]. The remaining oxygen that cannot be eliminated through the curing process can play an important role in decreasing the graphene nucleation density [20]. According to [21], almost all metal (except noble metals) may have deterioration while exposed to corroding environment. Some researchers also stated that there are many other factors that also affect the occurrence of corrosion process on metals such as temperature, pollutants, humidity, winds carrying chloride ions, rapid change in climate conditions, pH, etc [22] [23]. Figure 9 shows that the oxygen content accumulates a lot in areas that have cracks or corrosion on CI.

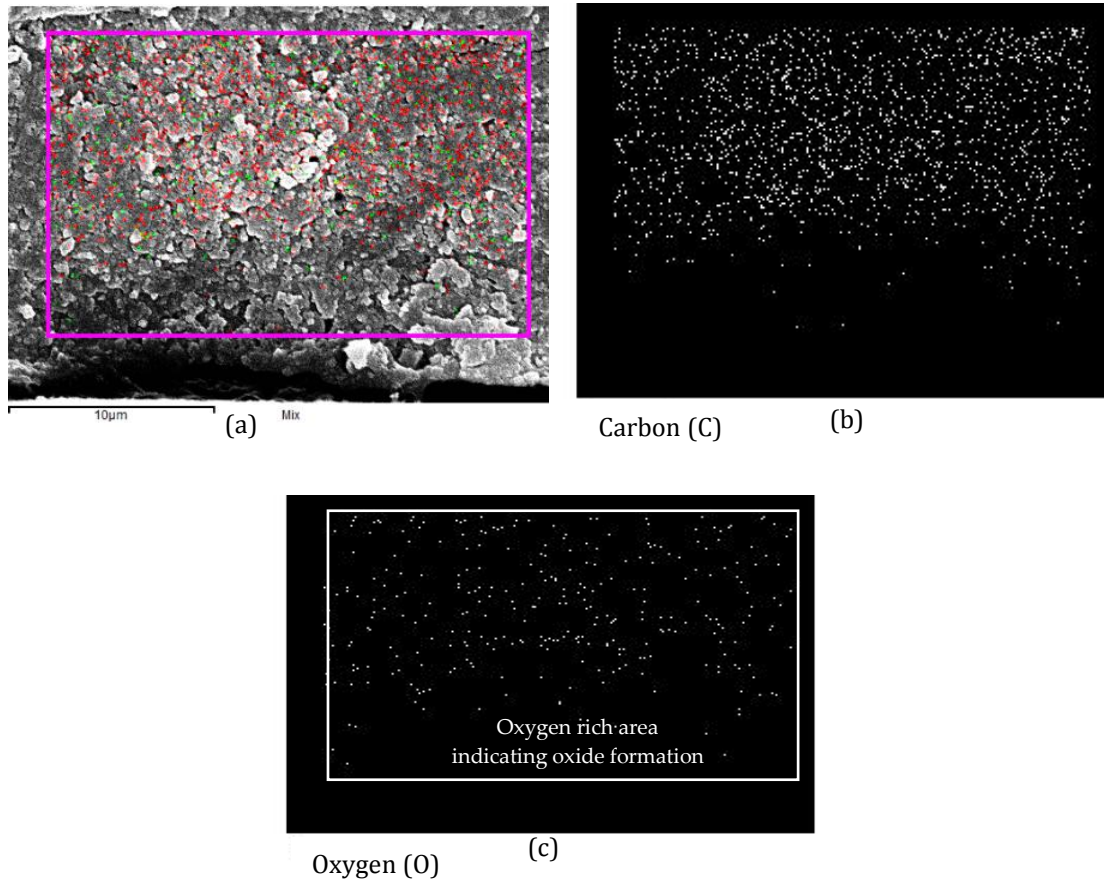


Figure 9: EDX Mapping Images with Oxygen Rich Area Indicating Oxide Formation of 20 Minutes Curing Time. (a) SEM Image, (b) EDX Mapping Image of Carbon (graphene), (c) EDX Mapping Image of Oxygen.

Since non-cohesive graphene causes several cracks during the 10-minute curing time, the oxygen content is uniformly distributed around the cross-section of the sample. It is evident that the oxygen atoms are present on the corroded surface indicating the formation of oxide layer [21].

4. CONCLUSION

The study was carried out successfully in demonstrating the comparative change in resistivity and elasticity caused by different filler loading curing times. Throughout the study, the findings suggest that curing times plays significant roles in determining the electrical conductivity, microstructure and mechanical performance of graphene. From the results, it clearly shows that electrical conductivity increases when the curing time increases. This is due to the graphene particle start to diffuse with each other when the curing time was increased, hence allowed smooth structure with less void. Therefore, this allows the electron to pass between each other with less resistance. The higher the graphene content, the more brittle the graphene becomes, resulting in more cracks and a loss of conductivity, as seen in Figure 8 when the curing time is extended after 30 minutes. Besides that, the graphene hardness increases after 30 minutes of curing time due to brittle grain boundaries of particles as the curing time increases. The sample with a curing time of 30 minutes has excellent electrical and mechanical properties, with high Young's modulus, low hardness, and low resistance. Showing that the filler loading was evenly distributed throughout the CI matrix with no obvious aggregation. SCI in-vehicle electronic equipment with low resistance and high elasticity would benefit the driver, allowing for more

effective monitoring of the driver's health. It's because SCI can be stretched to fit the shape of the human body and has good conductivity for measuring pulse and muscle movement.

REFERENCES

- [1] Zhang, B., Lei, J., Qi, D., Liu, Z., Wang, Y., Xiao, G., & Chen, X. Stretchable conductive fibers based on a cracking control strategy for wearable electronics. *Advanced Functional Materials*, **28**(29), (2018) pp.1801683.
- [2] Matsuhisa, N., Kaltenbrunner, M., Yokota, T., Jinno, H., Kuribara, K., Sekitani, T., & Someya, T. Printable elastic conductors with a high conductivity for electronic textile applications. *Nature communications*, **6**(1), (2015) pp.1-11.
- [3] Kedambaimoole, V., Neella, N., Gaddam, V., Rajanna, K., & Nayak, M. M. Graphene-Nickel composite films on flexible PCB for temperature monitoring. In *2017 IEEE 12th International Conference on Nano/Micro Engineered and Molecular Systems (NEMS)*, (2017) pp.173-176).
- [4] Xue, G., Zhang, B., Sun, M., Zhang, X., Li, J., Wang, L., & Song, C. Morphology, thermal and mechanical properties of epoxy adhesives containing well-dispersed graphene oxide. *International Journal of Adhesion and Adhesives*, **88**, (2019) pp.11-18.
- [5] Tran, T. S., Dutta, N. K., & Choudhury, N. R. Graphene inks for printed flexible electronics: Graphene dispersions, ink formulations, printing techniques and applications. *Advances in colloid and interface science*, **261**, (2018) pp.41-61.
- [6] Pan, K., Fan, Y., Leng, T., Li, J., Xin, Z., Zhang, J., & Hu, Z. Sustainable production of highly conductive multilayer graphene ink for wireless connectivity and IoT applications. *Nature communications*, **9**(1), (2018) pp.1-10.
- [7] AK Ab Wahid, MA Salim, M Ali, NA Masripan, F Dai & AM Saad. Measurement of Optimal Stretchability Graphene CI Pattern by Numerical Analysis. *Defence S&T Technical Bulletin* **14**(1), (2021) pp. 43-54.
- [8] Bourlier, Y., Noël, S., Viel, P., Brézard-Oudot, A., Chrétien, P., Franchini, A., & Karam, A. F. Characterization of Nanocomposite Graphene/polymer Films for Electrical Contact Applications. In *2018 IEEE Holm Conference on Electrical Contacts*. (2018) pp.448-455.
- [9] Arapov, K., Rubingh, E., Abbel, R., Laven, J., de with, G., & Friedrich, H. Conductive screen printing inks by gelation of graphene dispersions. *Advanced Functional Materials*, **26**(4), (2016) pp.586-593.
- [10] Wang, W., Peng, Q., Dai, Y., Qian, Z., & Liu, S. Distinctive nanofriction of graphene coated copper foil. *Computational Materials Science*, **117**, (2016) pp.406-411.
- [11] Batakliiev, T., Georgiev, V., Ivanov, E., Kotsilkova, R., Di Maio, R., Silvestre, C., & Cimmino, S. Nanoindentation analysis of 3D printed poly (lactic acid)-based composites reinforced with graphene and multiwall carbon nanotubes. *Journal of Applied Polymer Science*, **136**(13), (2019) 47260.
- [12] Compton, B. G., Hmeidat, N. S., Pack, R. C., Heres, M. F., & Sangoro, J. R. Electrical and mechanical properties of 3D-printed graphene-reinforced epoxy. *Jom*, **70**(3), (2018) pp.292-297.
- [13] Li, J., Ye, F., Vaziri, S., Muhammed, M., Lemme, M. C., & Östling, M. Efficient inkjet printing of graphene. *Advanced materials*, **25**(29), (2013) pp.3985-3992.
- [14] Gao, Y., Shi, W., Wang, W., Leng, Y., & Zhao, Y. Inkjet printing patterns of highly conductive pristine graphene on flexible substrates. *Industrial & engineering chemistry research*, **53**(43), (2014) pp.16777-16784.
- [15] Yunos, A. M., Omar, G., Salim, M. A., Masripan, N. A., & Al-Mola, M. H. A. The Effect of Temperature on the Electrical Conductivity and Microstructure Behaviour of Silver Particles. *International Journal of Nanoelectronics and Materials*, **13**, (2020) pp.431-438.
- [16] Karim, N., Zhang, M., Afroj, S., Koncherry, V., Potluri, P., & Novoselov, K. S. Graphene-based surface heater for de-icing applications. *RSC Advances*, **8**(30), (2018) pp.16815-16823.

- [17] Oliver, W. C., & Pharr, G. M. An improved technique for determining hardness and elastic modulus using load and displacement sensing indentation experiments. *Journal of materials research*, **7**(6), (1992) pp.1564-1583.
- [18] Mohammed, A.A. *Development of a New Stretchable and Screen Printable CI*, Doctoral dissertation, University of Maryland, Maryland. (2017.)
- [19] Li, J., Shao, L., Zhou, X., & Wang, Y. Fabrication of high strength PVA/rGO composite fibers by gel spinning. *Rsc Advances*, **4**(82), (2014) pp.43612-43618.
- [20] Ding, D., Solís-Fernández, P., Yunus, R. M., Hibino, H., & Ago, H. Behavior and role of superficial oxygen in Cu for the growth of large single-crystalline graphene. *Applied Surface Science*, **408**, (2017) pp.142-149.
- [21] Hikku, G. S., Jeyasubramanian, K., Venugopal, A., & Ghosh, R. Corrosion resistance behaviour of graphene/polyvinyl alcohol nanocomposite coating for aluminium-2219 alloy. *Journal of Alloys and Compounds*, **716**, (2017) pp.259-269.
- [22] Wu, H. C., Yang, B., Wang, S. L., Zhang, M. X., Shi, Y. Z., Chen, Y. F., & Sun, Y. H. Effect of thermal aging on corrosion fatigue of Z3CN20. 09M duplex stainless steel in high temperature water. *Materials Science and Engineering: A*, **655**, (2016) pp.183-192.
- [23] Liu, Z. Y., Wang, X. Z., Du, C. W., Li, J. K., & Li, X. G. Effect of hydrogen-induced plasticity on the stress corrosion cracking of X70 pipeline steel in simulated soil environments. *Materials Science and Engineering: A*, **658**, (2016) pp.348-354.